Acta Crystallographica Section A
Foundations of Crystallography
ISSN 0108-7673

Received 29 November 2008
Accepted 2 March 2009

Depth profiling of polymer films with grazing-incidence small-angle X-ray scattering

Marsha A. Singh* and Michael N. Groves

Physics, Engineering Physics and Astronomy, Queen's University, Stirling Hall, Kingston, Ontario, Canada K7L 3N6. Correspondence e-mail: singh@physics.queensu.ca

A model-free method of reconstructing depth-specific lateral scattering from incident-angle-resolved grazing-incidence small-angle X-ray scattering (GISAXS) data is proposed. The information on the material which is available through variation of the X-ray penetration depth with incident angle is accessed through reference to the reflected branch of the GISAXS process. Reconstruction of the scattering from lateral density fluctuations is achieved by solving the resulting Fredholm integral equation with minimal *a priori* information about the experimental system. Results from simulated data generated for hypothetical multilayer polymer systems with constant absorption coefficient are used to verify that the method can be applied to cases with large X-ray penetration depths, as typically seen with polymer materials. Experimental tests on a spin-coated thick film of a blend of diblock copolymers demonstrate that the approach is capable of reconstruction of the scattering from a multilayer structure with the identification of lateral scattering profiles as a function of sample depth.

1. Introduction

Surfaces and interfaces play an essential role in an ever-increasing range of technologically important materials. While direct probes such as atomic force microscopy (AFM) and scanning tunnelling microscopy (STM) can offer effective characterization of both surface (Leroy *et al.*, 2008; Fruchart *et al.*, 2003) and below-surface (Dietz *et al.*, 2008) structures, the resulting information is generally limited to small areas and does not readily provide access to statistically averaged quantities, which are often necessary to compile a complete picture of static and dynamic properties. X-ray techniques have been shown to be ideal tools (Foster, 1993) for the characterization of structure parallel and perpendicular to surfaces and interfaces. Grazing-incidence X-ray diffraction (GIXD) (David *et al.*, 2008; Heo *et al.*, 2008; Robinson *et al.*, 2005) and X-ray reflectivity (XRR) (Fenter & Park, 2004) are established tools for the measurement of laterally homogeneous material structure normal to the surface. Grazing-incidence small-angle X-ray scattering (GISAXS) offers access to scattering information in the plane of the surface (Lee *et al.*, 2008, 2007; Lee, Park *et al.*, 2005; Busch *et al.*, 2007; Lee, Yoon *et al.*, 2005; Müller-Buschbaum, 2003), relative to both the direct and, for the correct choice of incident angle with a dense substrate supporting a film of the material, the reflected beams.

Both GIXD and GISAXS have often been applied to obtain qualitative depth-profiling measurements through variation of the incident and exit angles (Stein *et al.*, 2007; Colombi *et al.*, 2007; Pfeiffer *et al.*, 2004; Ferrero *et al.*, 2003; Gibaud *et al.*, 2003; Neerinck & Vink, 1996) to control the penetration depth in the sample. When either or both of the incident or exit angles are below the critical angle at the air–material interface, the radiation probe is confined to the surface layer down to a depth of the order of 10 nm. At higher angles, the scattering depth can extend to microns, well into the bulk phase or supporting substrate. The resulting scattering information represents a cumulative average of the scattering seen over the full range of material encountered by the X-rays. An alternative approach to obtaining true depth-specific scattering information has been suggested by Reichert *et al.* (2003), relying on high-energy X-ray microbeams to directly probe material layers at different depths below the surface by impinging on the sample from one side. Fruchart *et al.* (2003) discuss the combined use of STM and GISAXS methods to separate surface from below-surface scattering information.

The possibility of obtaining true depth-specific information from conventional X-ray diffraction measurements has been addressed in recent reports (Kötschau & Schock, 2006; Broadhurst, Rogers, Lowe & Lane, 2005; Broadhurst, Rogers, Lane & Lowe, 2005). In this work, the method of Broadhurst, Rogers, Lowe & Lane (2005), which employs a model-independent numerical method of resolving scattering information specific to varying depths below the surface, is applied to GISAXS data. The desired result from data obtained using a series of incident angles is a reconstruction of the lateral or in-plane scattering from specific depths below the surface. The theoretical foundation of the proposed procedure for GISAXS applications is first outlined. The numerical approach is formulated and tested on simulated data gener-

ated from hypothetical multilayer systems with well defined in-plane electron-density inhomogeneity. The method is then extended to a test-case study of experimental GISAXS data from a blend of two immiscible diblock copolymers spin-coated onto a silicon substrate. The copolymer blend was chosen as a test system since it exhibits both macro- and microphase separation, thereby creating a multilayered system with distinct lateral structures characterizing the different layers.

Block copolymers have long been recognized as having great potential for the fabrication of organized nanostructures and devices (Metwalli *et al.*, 2008; Hamley, 1998). The phenomenon of self-ordering, driven by the incompatibility of unlike polymer segments, offers an ideal alternative to top-down manufacturing methods for nanoscale devices. The bulk microstructures of these materials have been well characterized using microscopy and small-angle scattering methods. However, it is well known that surface microstructure and mobility effects can differ significantly from the bulk case and will vary with depth below the surface (Kitano *et al.*, 2007; Kawaguchi *et al.*, 2003; Brown & Chakrabarti, 1994). The extent to which surface effects are manifested below the air–polymer interface is not well established. It is reasonable to expect that the presence of physical and/or chemical cross-linking in a highly entangled system of long-chain molecules would extend surface effects well beyond the size of a single molecule. A detailed understanding of depth-dependent static and dynamic properties is essential to the development of highly functionalized materials. These considerations are the driving force behind the current effort to apply depth-profiling procedures such as that proposed by Broadhurst, Rogers, Lowe & Lane (2005) to thick polymer films. It is anticipated that the preliminary results reported here can be extended to development of depth-dependent phase diagrams of copolymer surfaces and measurement of the ordering kinetics seen in response to thermal quenching (Singh *et al.*, 2007) between distinct copolymer phases at specific depths below the surface.

2. Theoretical foundation

2.1. GISAXS basic formulae

The basic setup of a GISAXS experiment referring to a medium of finite thickness supported on a semi-infinite substrate is sketched in Fig. 1. It is assumed that three media [air/vacuum, medium (m), substrate (s)] exist with relative indices of refraction $n_{\rm air} < n_{\rm m} < n_{\rm s}$. The theoretical formulation of GISAXS derived recently (Lee, Park *et al.*, 2005; Lee *et al.*, 2007; Lee, Yoon *et al.*, 2005) is briefly reviewed here to establish the conceptual basis for the depth-profiling procedure.

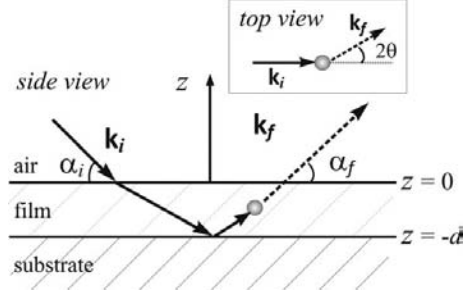

Figure 1
GISAXS geometry showing one of four possible branches of scattering.

For an incident plane wave of wavevector $\mathbf{k}_{\rm i}$ and exit plane wave with wavevector $\mathbf{k}_{\rm f}$, the boundary conditions imposed by Maxwell's equations yield two solutions (Lee *et al.*, 2007; Dosch, 1992) for the electric field inside a uniform medium at $\mathbf{r}$, where the medium of thickness d is bounded above by the vacuum and below by the substrate,

$$\begin{aligned}\Psi_{\rm i}(\mathbf{k}_{\rm i},\mathbf{r}) &= \exp\left(i\mathbf{k}_{||,{\rm i}}\cdot\mathbf{r}_{||}\right)\left[T_{\rm i}\exp\left(i\tilde{k}_{z,{\rm i}}z\right)+R_{\rm i}\exp\left(-i\tilde{k}_{z,{\rm i}}z\right)\right],\\ \Psi_{\rm f}(\mathbf{k}_{\rm f},\mathbf{r}) &= \exp\left(i\mathbf{k}_{||,{\rm f}}\cdot\mathbf{r}_{||}\right)\left[T_{\rm f}^{*}\exp\left(i\tilde{k}_{z,{\rm f}}^{*}z\right)+R_{\rm f}^{*}\exp\left(-i\tilde{k}_{z,{\rm f}}^{*}z\right)\right],\\ &\quad 0>z>-d. \end{aligned} \tag{1}$$

Following Lee *et al.* (2007), $\mathbf{r} = (\mathbf{r}_{||}, z)$, $\mathbf{k}_{||}$ is the wavevector component parallel to the interface, $\tilde{k}_{z,j}$ (with j = i, f) is the refracted component of the wavevector normal to the interface, and the amplitudes of the transmitted and reflected waves inside the medium are given by the Fresnel coefficients T_j and R_j. As usual, * indicates the complex conjugate. Conventional X-ray reflectivity information associated with substrate-supported homogeneous films is not accounted for in this formulation.

The above solutions are exact for smooth interfaces bounding a uniform medium with electron density $\bar{\rho}$. If it is assumed that the medium includes local deviations in electron density that are sufficiently small to be treated as perturbations, the electron density is written as $\rho(\mathbf{r}) = \bar{\rho} + \Delta\rho(\mathbf{r})$. The deviations $\Delta\rho(\mathbf{r})$ give rise to a scattering potential (Lee *et al.*, 2007; Born & Wolf, 1999) $V(\mathbf{r}) = vr_o\Delta\rho(\mathbf{r})$, where v is the total volume occupied by $\Delta\rho(\mathbf{r})$ and r_o is the classical electron radius (Als-Nielsen & McMorrow, 2001). In the first-order Born approximation, the scattering amplitude for $\mathbf{q} = \mathbf{k}_{\rm f} - \mathbf{k}_{\rm i}$ at a distance R far from the scattering region is given by

$$\Psi_{\rm sc}(\mathbf{q},R) = -\{[\exp(ikR)]/R\}\int_V {\rm d}\mathbf{r}\,\Psi_{\rm f}^{*}(\mathbf{r})V(\mathbf{r})\Psi_{\rm i}(\mathbf{r}), \tag{2}$$

where k is the magnitude of the wavevector ($k = |\mathbf{k}_{\rm i}| = |\mathbf{k}_{\rm f}|$) and the integration is over the volume of the medium.

As noted by numerous authors (Lee, Park *et al.*, 2005; Lee *et al.*, 2007; Vartanyants *et al.*, 2007; Lee, Yoon *et al.*, 2005), when the incident angle $\alpha_{\rm i}$ is greater than the air–medium critical angle, $\alpha_{\rm c,m}$, the total scattered wave amplitude can be written as the sum of four distinct scattering amplitudes resulting from the product of terms in equation (2). For the current case of a medium of finite thickness supported by a semi-infinite substrate (Lee, Park *et al.*, 2005; Lee *et al.*, 2007; Lee, Yoon *et al.*, 2005), this sum has been shown to be

$$\begin{aligned}\Psi_{\rm sc}(\mathbf{q},R) = -\{[\exp(ikR)]/R\}\int_V {\rm d}\mathbf{r}\,\exp(-i\mathbf{q}_{||}\cdot\mathbf{r}_{||})V(\mathbf{r})\\ \times\left[T_{\rm i}T_{\rm f}\exp(-iq_{1,z}z)+T_{\rm i}R_{\rm f}\exp(-iq_{2,z}z)\right.\\ \left.+R_{\rm i}T_{\rm f}\exp(-iq_{3,z}z)+R_{\rm i}R_{\rm f}\exp(-iq_{4,z}z)\right],\end{aligned} \tag{3}$$

where $\mathbf{q}_{||} = \mathbf{k}_{||,\mathrm{f}} - \mathbf{k}_{||,\mathrm{i}}$ is the in-plane momentum transfer vector. The individual z components of the momentum transfer inside the medium, $q_{1,z} = \tilde{k}_{z,\mathrm{f}} - \tilde{k}_{z,\mathrm{i}}$, $q_{2,z} = -\tilde{k}_{z,\mathrm{f}} - \tilde{k}_{z,\mathrm{i}}$, $q_{3,z} = \tilde{k}_{z,\mathrm{f}} + \tilde{k}_{z,\mathrm{i}}$ and $q_{4,z} = -\tilde{k}_{z,\mathrm{f}} + \tilde{k}_{z,\mathrm{i}}$, are identified with specific scattering processes by noting the condition yielding $q_{i,z} = 0$. In the case of $q_{2,z}$ and $q_{3,z}$, this occurs when $\tilde{k}_{z,\mathrm{f}} = -\tilde{k}_{z,\mathrm{i}}$, indicating scattering about the reflected beam (Stein *et al.*, 2007; Lee, Park *et al.*, 2005). Similarly, $q_{1,z}$ and $q_{4,z}$ are identified as representing scattering about the direct beam. Since $q_{1,z} = -q_{4,z}$ and $q_{2,z} = -q_{3,z}$, the GISAXS amplitude may be identified as being the sum of two sets of scattering events about the direct and reflected beams.

Assuming that the cross terms resulting from the product of equation (2) can be neglected (Lee, Park *et al.*, 2005; Lee, Yoon *et al.*, 2005) and that the incident angle is greater than the air–medium critical angle, the observed intensity is effectively the sum of two distinct sets of scattering events by the direct ($\tilde{k}_{z,\mathrm{i}}$) and reflected ($-\tilde{k}_{z,\mathrm{i}}$) sources. In this work it is assumed that these scattering events can be distinguished in the measured GISAXS data (Lee, Park *et al.*, 2005) and only the results of scattering from the reflected beam will be considered. In addition, it will be assumed that consideration can be restricted to $q_{3,z}$ terms only. As described previously (Stein *et al.*, 2007), scattering associated with $q_{2,z}$ occurs before specular reflection from the substrate while scattering associated with $q_{3,z}$ occurs after specular reflection. Ideally, GISAXS experiments relying on the reflected beam use an incident angle within the range $\alpha_{\mathrm{c,m}} < \alpha_{\mathrm{i}} < \alpha_{\mathrm{c,s}}$, where $\alpha_{\mathrm{c,s}}$ is the critical angle of the substrate. Given that the materials of interest are assumed to be weak scatterers within the Born approximation, the large path lengths introduced by the shallow incident and exit angles of a typical GISAXS experiment imply that scattering associated with $q_{2,z}$ will be negligible in comparison to scattering occurring *after* specular reflection ($q_{3,z}$). In the latter case, absorption of the scattered radiation takes place only on the path out of the sample towards the detector (Lee, Yoon *et al.*, 2005). With these assumptions in place, the scattered wave amplitude of interest, $\Psi_{\mathrm{sc}}^{\Re}$, is

$$\begin{aligned}\Psi_{\mathrm{sc}}^{\Re}(\mathbf{q}, R) &= -\{[vr_o \exp(ikR)]/R\} R_{\mathrm{i}} T_{\mathrm{f}} \int_V \mathrm{d}\mathbf{r}\, \Delta\rho(\mathbf{r}_{||}, z) \\ &\quad \times \exp(-i\mathbf{q}_{||} \cdot \mathbf{r}_{||}) \exp(-iq_{3,z} z) \\ &= -\{[vr_o \exp(ikR)]/R\} R_{\mathrm{i}} T_{\mathrm{f}} F^{\Re}(\mathbf{q}), \end{aligned} \tag{4}$$

where $F^{\Re}(\mathbf{q})$ represents the kinematic structure amplitude associated with the specific branch of GISAXS given by the momentum transfer $q_{3,z}$.

For incident radiation of wavelength λ the momentum transfer ($\mathbf{q}_{||}$, $q_{3,z}$) inside the medium for the specific scattering process of interest has components (Dosch, 1992)

$$\begin{aligned} q_x &= (2\pi/\lambda)(\cos 2\theta \cos\tilde{\alpha}_{\mathrm{f}} - \cos\tilde{\alpha}_{\mathrm{i}}), \\ q_y &= (2\pi/\lambda)(\sin 2\theta \cos\tilde{\alpha}_{\mathrm{f}}), \\ q_{3,z} &= (2\pi/\lambda)(-\sin\tilde{\alpha}_{\mathrm{f}} + \sin\tilde{\alpha}_{\mathrm{i}}). \end{aligned} \tag{5}$$

Following the convention defined in Fig. 1, α_{i} and α_{f} are the incident and exit angles relative to the interface in the (xy) plane, $\tilde{\alpha}_{\mathrm{i}}$ and $\tilde{\alpha}_{\mathrm{f}}$ are the refracted incident and exit angles seen inside the medium, and 2θ is the horizontal scattering angle (no refraction). Rewriting $q_{3,z}$ in terms of the directly measured quantities, α_{i} and α_{f}, for a medium of uniform index of refraction, $n_{\mathrm{m}} = 1 - \delta_{\mathrm{m}} + i\beta_{\mathrm{m}}$ (Als-Nielsen & McMorrow, 2001),

$$\begin{aligned} q_{3,z} = (2\pi/\lambda)\big[&-(\sin^2\alpha_{\mathrm{f}} - 2\delta_{\mathrm{m}} + 2i\beta_{\mathrm{m}})^{1/2} \\ &+ (\sin^2\alpha_{\mathrm{i}} - 2\delta_{\mathrm{m}} + 2i\beta_{\mathrm{m}})^{1/2}\big]. \end{aligned} \tag{6}$$

The scattering depth describing the interaction range of the X-ray probe inside the medium is given by the inverse of the imaginary component of $q_{3,z}$ (Lee, Yoon, *et al.*, 2005; Dosch, 1992),

$$\Lambda \equiv |\mathrm{Im}(q_{3,z})|^{-1} = \lambda/[2\pi(l_{\mathrm{i}} + l_{\mathrm{f}})], \tag{7}$$

$$l_{\mathrm{i,f}} = 2^{-1/2}\left\{(2\delta_{\mathrm{m}} - \sin^2\alpha_{\mathrm{i,f}}) - \left[(\sin^2\alpha_{\mathrm{i,f}} - 2\delta_{\mathrm{m}})^2 + 4\beta_{\mathrm{m}}^2\right]^{1/2}\right\}^{1/2}.$$

With the real part of $q_{3,z}$ written as $Q_z \equiv \mathrm{Re}(q_{3,z})$, the scattering amplitude is written as

$$\begin{aligned} F^{\Re}(\mathbf{q}) &= \int_{-d}^{0} \mathrm{d}z \int \mathrm{d}\mathbf{r}_{\|}\, \Delta\rho(\mathbf{r}_{||}, z) \exp(-i\mathbf{q}_{||} \cdot \mathbf{r}_{||}) \\ &\quad \times \exp(-iQ_z z) \exp(-z/\Lambda) \\ &= \int_{-d}^{0} \mathrm{d}z\, F_{||}^{\Re}(\mathbf{q}_{||}, z) \exp(-iQ_z z) \exp(-z/\Lambda), \end{aligned} \tag{8}$$

where $F_{||}^{\Re}(\mathbf{q}_{||}, z)$ represents the in-plane structure amplitude at a position (depth) z inside the medium (Dosch, 1992).

Finally, the observed intensity of that part of the GISAXS profile under consideration is proportional to the absolute square of the scattered wave amplitude,

$$\begin{aligned} I^{\Re}(\mathbf{q}) &\propto |R_{\mathrm{i}} T_{\mathrm{f}}|^2 |F^{\Re}(\mathbf{q})|^2 \\ &= |R_{\mathrm{i}} T_{\mathrm{f}}|^2 \left| \int_{-d}^{0} \mathrm{d}z\, F_{||}^{\Re}(\mathbf{q}_{||}, z) \exp(-iQ_z z) \exp(-z/\Lambda) \right|^2. \end{aligned} \tag{9}$$

Consider now a representation of the integral for the structure amplitude over z in discretized form, summing over layers of finite thickness, Δz, with N layers extending from $-d < z < 0$. In each layer, located at $z = z_j$, the ratio z_j/Λ is written as a constant and the possibility of an index of refraction varying with depth is neglected as a first-order approximation. The thickness Δz is chosen to be sufficiently large to give access to structural information within the layer and, as discussed later, to allow for incoherent addition of scattering amplitudes from different layers (Luo & Tao, 1996). It should be noted that this construction is not intended to apply to a discrete layer system with sharp interfaces (Lee, Yoon *et al.*, 2005). The scattering amplitude becomes

$$F^{\Re}(\mathbf{q}) \simeq \Delta z \sum_{j=1}^{N} \exp(-z_j/\Lambda) \left[\int_{z_j}^{z_{j+1}} \mathrm{d}z' F_{||}^{\Re}(\mathbf{q}_{||}, z') \exp(-iQ_z z') \right]. \tag{10}$$

The observed intensity can therefore be written as the sum over independent scattering contributions from the individual

layers, weighted by the absorption terms, and the cross terms arising from the products of structure amplitudes of different layers.

$$I^{\Re}(\mathbf{q}) \propto |R_i T_f|^2 \left| \sum_{j=1}^{N} \exp(-z_j/\Lambda) \left[\int_{z_j}^{z_{j+1}} dz' F_{||}^{\Re}(\mathbf{q}_{||}, z') \exp(-iQ_z z') \right] \right|^2$$
$$= |R_i T_f|^2 \left[\sum_{j=1}^{N} \exp(-2z_j/\Lambda) I_j^{\Re}(\mathbf{q}_{||}, Q_z, z_j) + I_{\text{cross}}^{\Re} \right]. \quad (11)$$

A rigorous theoretical treatment dealing with the role played by the cross terms will not be attempted in this work. Instead, it will be assumed that for the applications of interest the intensity contribution from the interference term, $I_{\text{cross}}^{\Re}$, may be neglected. That is, a minimum layer thickness, Δz, is chosen to allow for incoherent summation of the scattering amplitudes from the layers at z_j (Luo & Tao, 1996). This situation may be realized when dealing with finite layer thickness in the absence of a highly coherent X-ray source with the assumption that the usual experimental difficulties associated with GISAXS measurements (Schlepütz *et al.*, 2005) have been successfully dealt with. The observed scattering about the reflected GISAXS beam is then simply expressed as the sum of scattering intensities from N layers, weighted by the absorption factor, $\exp(-2z_j/\Lambda)$.

The final expression for the GISAXS relative to the reflected beam can be compared to similar integral formulations that have been used in depth-resolved X-ray diffraction analysis (Broadhurst, Rogers, Lowe & Lane, 2005; Luo & Tao, 1996) and early reports on the application of GISAXS methods to the study of thin surface layers (Naudon *et al.*, 1991). For the simple case of a material with a constant linear absorption coefficient μ ($\mu = 2k\beta_m$) referring to intensity attenuation rather than amplitude attenuation (Als-Nielsen & McMorrow, 2001), the observed X-ray diffraction intensity (Broadhurst, Rogers, Lowe & Lane, 2005) can be written as

$$I^{\text{obs}}(\alpha_i, 2\theta_d) \propto \int_{-d}^{0} dz\, I(z, \theta_d) \exp\left\{ -\mu z \left[\frac{1}{\sin\alpha_i} + \frac{1}{\sin(2\theta_d - \alpha_i)} \right] \right\}. \quad (12)$$

In equation (12), α_i is again the angle of incidence relative to the sample surface and $2\theta_d$ is the scattering angle in the plane of incidence relative to the direct beam. Diffraction data from the medium at depth z, $I(z, \theta_d)$, are recovered. Broadhurst, Rogers, Lowe & Lane (2005) assumed that the medium was homogeneous in the direction parallel to the interface throughout the depth of the sample. For the purposes of this work, the procedure outlined by Broadhurst, Rogers, Lowe & Lane (2005) is adapted to deal with GISAXS data obtained for varying incident angle, α_i, typically using two-dimensional detection giving access to scattering information as a function of both $2\theta_d$ (alternatively α_f) and $\mathbf{q}_{||}$. In particular, information regarding variations of in-plane scattering as a function of depth below the sample surface is desired. The present goal is therefore reconstruction of scattering information $I(\mathbf{q}_{||}, z)$ from specific depths z below the sample surface for fixed Q_z. It must be noted that the condition of fixed Q_z generally implies variation of α_f with varying α_i [$Q_z \equiv \text{Re}(q_3, z)$, where $q_{3,z}$ is given in equation (6)]. In accordance with the basic premise of the depth-profiling algorithm, the scattering depth $\Lambda(\alpha_i, \alpha_f)$ will vary with α_i when Q_z is held fixed. The original procedure proposed by Broadhurst, Rogers, Lowe & Lane (2005) can, of course, still be applied to obtain information of the form $I(Q_z, z)$ for fixed $\mathbf{q}_{||}$.

2.2. Depth-profiling algorithm

Equation (11), written now in integral form with $I_{\text{cross}}^{\Re}$ neglected, can be used as the starting point for applying the numerical methods proposed by Broadhurst, Rogers, Lowe & Lane (2005) to extract intensities $I^{\Re}(\mathbf{q}_{||}, Q_z, z)$ from the measured scattering profiles obtained for a range of α_i values. Including geometric factors associated with the beam cross section on the sample and explicit reference to the angle of incidence, equation (11) is rewritten as

$$I^{\Re}(\alpha_i, \mathbf{q}_{||}, Q_z) \simeq \left(|R_i T_f|^2 / \sin\alpha_i \right) \times \int_{-d}^{0} dz\, \exp(-2z/\Lambda) I^{\Re}(\mathbf{q}_{||}, Q_z, z). \quad (13)$$

The intensity contribution, $I^{\Re}(\mathbf{q}_{||}, Q_z, z)$, is a function only of the scattering power for the below-surface layer at z for the momentum transfer, $(\mathbf{q}_{||}, Q_z)$, independent of the α_i geometrical factor. The scattering depth for the layer at a depth z, $\Lambda(\alpha_i, \alpha_f)$, is a function of incident and exit angle relative to the air–material interface and can be written as $\Lambda(\alpha_i, Q_z)$. In the following discussion it is assumed that the measured GISAXS data are processed to account for parasitic background and the $|R_i T_f|^2/\sin\alpha_i$ prefactor in equation (13). For fixed $(\mathbf{q}_{||}, Q_z)$ equation (13) can then be identified as a standard Fredholm integral equation of the first kind (Broadhurst, Rogers, Lowe & Lane, 2005) with a kernel given by $K(z, \alpha_i) = \exp(-2z/\Lambda)$. The observed scattering intensity measured for varying incident angle α_i can then be written as

$$I^{\text{obs}}(\alpha_i) \simeq \int_{-d}^{0} dz\, K(z, \alpha_i) I^{o}(z). \quad (14)$$

The notation used here is intended to follow that of Broadhurst, Rogers, Lowe & Lane (2005) in referring to $I^{\Re}(\alpha_i, \mathbf{q}_{||}, Q_z)$ and $I^{\Re}(\mathbf{q}_{||}, Q_z, z)$ as $I^{\text{obs}}(\alpha_i)$ and $I^{o}(z)$, respectively. Recovery of the scattering for a given value of $(\mathbf{q}_{||}, Q_z)$ from the medium at a depth z below the sample surface, $I^{o}(z)$, is the goal of the depth-profiling procedure.

Inverting integrals of the form given in equation (14) is known to be complicated by the fact that small perturbations in the measured quantity, $I^{\text{obs}}(\alpha_i)$, can lead to large distortions in the recovered values for $I^{o}(z)$ (Svergun, 1992; Broadhurst, Rogers, Lowe & Lane, 2005). Broadhurst, Rogers, Lowe & Lane (2005) have proposed a numerical method of determining $I^{o}(z)$ as a linear combination of n Chebyshev polynomials, $T_j(z)$, using the method of collocation (Boyce & DiPrima, 1997).

Following Broadhurst, Rogers, Lowe & Lane (2005), $I^{o}(z)$ is written as

$$I^o(z) = \sum_{j=1}^{n} a_j T_j(z)$$
$$T_1(z) = 1,$$
$$T_2(z) = (2z/d) - 1, \ldots,$$
$$T_n(z) = 2[(2z/d) - 1]T_{n-1}(z) - T_{n-2}(z). \quad (15)$$

According to the method of collocation, values for $I^o(z)$ are calculated at depth values z that coincide with the zeros of the nth Chebyshev polynomial,

$$z_j^o = \left(\frac{d}{2}\right)\left\{\cos\left[\frac{(2j-1)\pi}{2(n-1)}\right] + 1\right\}, \quad j = 1, 2, \ldots, n. \quad (16)$$

This approach is applied to ensure the best fit of equation (14) for the observed data (after processing as noted above) at all α_i values. Values for the scattering intensity for fixed ($\mathbf{q}_\parallel$, Q_z) momentum transfer are thereby determined at specific depth locations, z_j^o. Defining the matrix $\mathbf{T}$ of values of the Chebyshev polynomials calculated for a medium of thickness d at the zeros of the nth Chebyshev polynomial, $T_i(z_j^o)$, the final solution of interest is written as

$$I^o(z_j^o) = \sum_{i=1}^{n} a_i T_i(z_j^o). \quad (17)$$

For m incident angles $\alpha_{i,k}$, $k = 1, \ldots, m$, equation (14) can be rewritten as

$$I^{\rm obs}(\alpha_{i,k}) \simeq \sum_{j=1}^{n} a_j \int_{-d}^{0} dz\, K(z, \alpha_{i,k}) T_j(z),$$

$$\begin{bmatrix} I^{\rm obs}(\alpha_{i,1}) \\ \vdots \\ I^{\rm obs}(\alpha_{i,m}) \end{bmatrix}$$
$$\simeq \begin{bmatrix} \int_{-d}^{0} dz\, K(z, \alpha_{i,1}) T_1(z) & \cdots & \int_{-d}^{0} dz\, K(z, \alpha_{i,1}) T_n(z) \\ \vdots & \ddots & \vdots \\ \int_{-d}^{0} dz\, K(z, \alpha_{i,m}) T_1(z) & \cdots & \int_{-d}^{0} dz\, K(z, \alpha_{i,m}) T_n(z) \end{bmatrix} \begin{bmatrix} a_1 \\ \vdots \\ a_n \end{bmatrix}$$
$$\text{or} \quad \underline{I}^{\rm obs} \simeq \mathbf{Z}\underline{a}. \quad (18)$$

The $m \times n$ matrix of definite integrals, $\mathbf{Z}$, is in general not square. Following the solution prescription outlined by Broadhurst, Rogers, Lowe & Lane (2005), the final goal of determining the vector of coefficients, $\underline{a}$, is achieved using linear regularization. They identify a residual function which incorporates a stabilizer that is the product of a regularization parameter, γ, and a function of the solution, $I^o(z)$. First-order regularization (Press *et al.*, 1992) is incorporated in the form of the $(n-1) \times n$ matrix $\mathbf{B}$, introduced below. The final result for the vector of coefficients $\underline{a}$ is the solution of the equations [see Broadhurst, Rogers, Lowe & Lane (2005) for details of the derivation]

$$\left(\mathbf{Z}^T\mathbf{Z} + \gamma\mathbf{T}^T\mathbf{B}^T\mathbf{B}\mathbf{T}\right)\underline{a} = \mathbf{Z}^T\underline{I}^{\rm obs}, \quad (19)$$

where

$$\mathbf{B} = \begin{pmatrix} -1 & 1 & 0 & \ldots & 0 & 0 \\ 0 & -1 & 1 & \ldots & 0 & 0 \\ \vdots & \vdots & \vdots & \ddots & \vdots & \vdots \\ 0 & 0 & 0 & \ldots & -1 & 1 \end{pmatrix},$$
$$\gamma = c\left[\frac{\mathrm{tr}(\mathbf{Z}^T\mathbf{Z})}{\mathrm{tr}(\mathbf{T}^T\mathbf{B}^T\mathbf{B}\mathbf{T})}\right]. \quad (20)$$

In equation (20) the value of the constant, c, is determined by a combination of the objective χ^2 criterion (Press *et al.*, 1992) and a subjective identification of a non-negative result with an acceptable degree of smoothness in the final solution (Svergun, 1992). Broadhurst, Rogers, Lowe & Lane (2005) report that a value of $c = 0.3$ worked well for their numerical experiments.

Finally, the solution to equation (19) yields the vector of coefficients, $\underline{a}$, which is used in equation (17) to calculate $I^o(z_j^o)$ for fixed ($\mathbf{q}_\parallel$, Q_z). The matrices of equation (19), $\mathbf{Z}$, $\mathbf{B}$ and $\mathbf{T}$, are independent of $\mathbf{q}_\parallel$. Therefore, for a given (fixed) value of Q_z, the calculation outlined in equation (19) can be straightforwardly repeated for each vector of observed intensities $I^{\rm obs}(\alpha_{i,k})$ at different $\mathbf{q}_\parallel$ to reconstruct the depth-specific scattering intensity in the horizontal plane, $I^o(z_j^o, \mathbf{q}_\parallel)$.

3. Application of the depth-profiling algorithm

In this section the proposed method of GISAXS depth profiling is applied to both simulated and experimental data using the *MATLAB* programming environment. The simulated systems consist of thick, thin and bilayer films without explicit reference to the multiple-scattering effects that must be considered for real substrate-supported films. That is, ideal conditions including the avoidance of reflectivity effects (Lee *et al.*, 2007) are assumed. The choice of model systems follows that of Broadhurst, Rogers, Lowe & Lane (2005) to provide a straightforward test of the validity of the modifications to the original numerical method described above. An application to an experimental test case of angle-resolved GISAXS data from a simple blend of diblock copolymers spin-coated onto a silicon substrate is used to assess the feasibility of the method for dealing with real systems. In all cases considered, the simplest condition of an approximately uniform absorption factor is assumed. The possibility of incorporating a variable absorption factor has been addressed for (wide-) angle-resolved X-ray diffraction (Broadhurst, Rogers, Lane & Lowe, 2005; Kötschau & Schock, 2006).

3.1. Simulated data

Simulated data were generated following the general prescription associated with scattering about the direct (transmitted across the air–material interface) beam (Naudon *et al.*, 1991) for three ideal test cases similar to those examined by Broadhurst, Rogers, Lowe & Lane (2005). A uniform absorption coefficient, $\mu = 2.5 \times 10^{-7}$ nm^{-1}, air–medium critical angle of 0.07°, X-ray wavelength of 0.119 nm and total film thickness, D, of 3 µm are assumed for all cases. An

incident-angle range of 0.0700–0.1650° with increments of 0.0025° was used to generate simulated data with the ideal q_y ($\mathbf{q}_{||}$) range of 0.01–1.00 nm^{-1}. Hypothetical scattering depths varied from about 195 nm to 1.06 × 10^4 nm. Ideal scattering was generated to simulate the appearance of a small-angle-scattering profile for a hypothetical system of particles with no long-range ordering using the sum of a Gaussian centred about the direct beam and a Lorentzian centred at q_y = 0.5 nm^{-1}. It is assumed that the scattering data were located at the specular location so that the requirement of fixed $Q_z = 0$ is automatically satisfied. Depth-resolved data were recovered using 40 terms (n = 40) in the Chebyshev polynomial series with the result that lateral scattering was constructed at 40 unevenly spaced locations within the sample depth. Depth profiling following the prescription outlined in §2.2 was performed assuming knowledge of the true absorption, μ, and

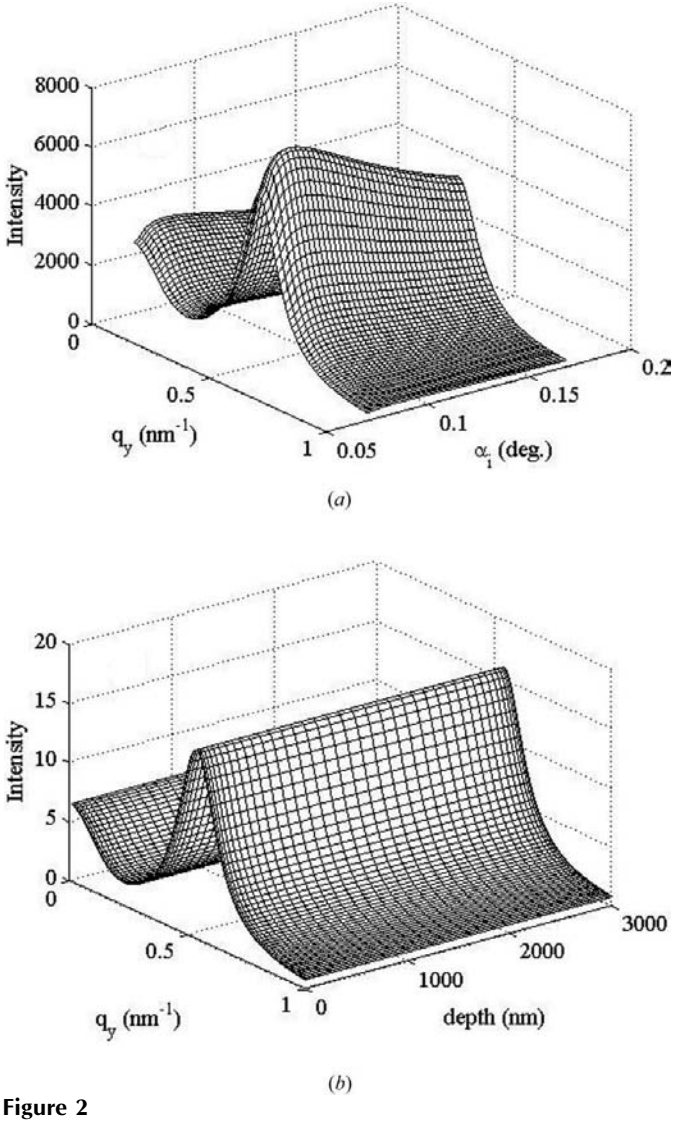

Figure 2
(*a*) Simulated GISAXS profiles for varying incident angles and a thick (3 µm) homogeneous film. (*b*) Reconstructed GISAXS profiles as a function of depth, $-z$, below the air–material interface. Arbitrary units are used for intensities in all figures.

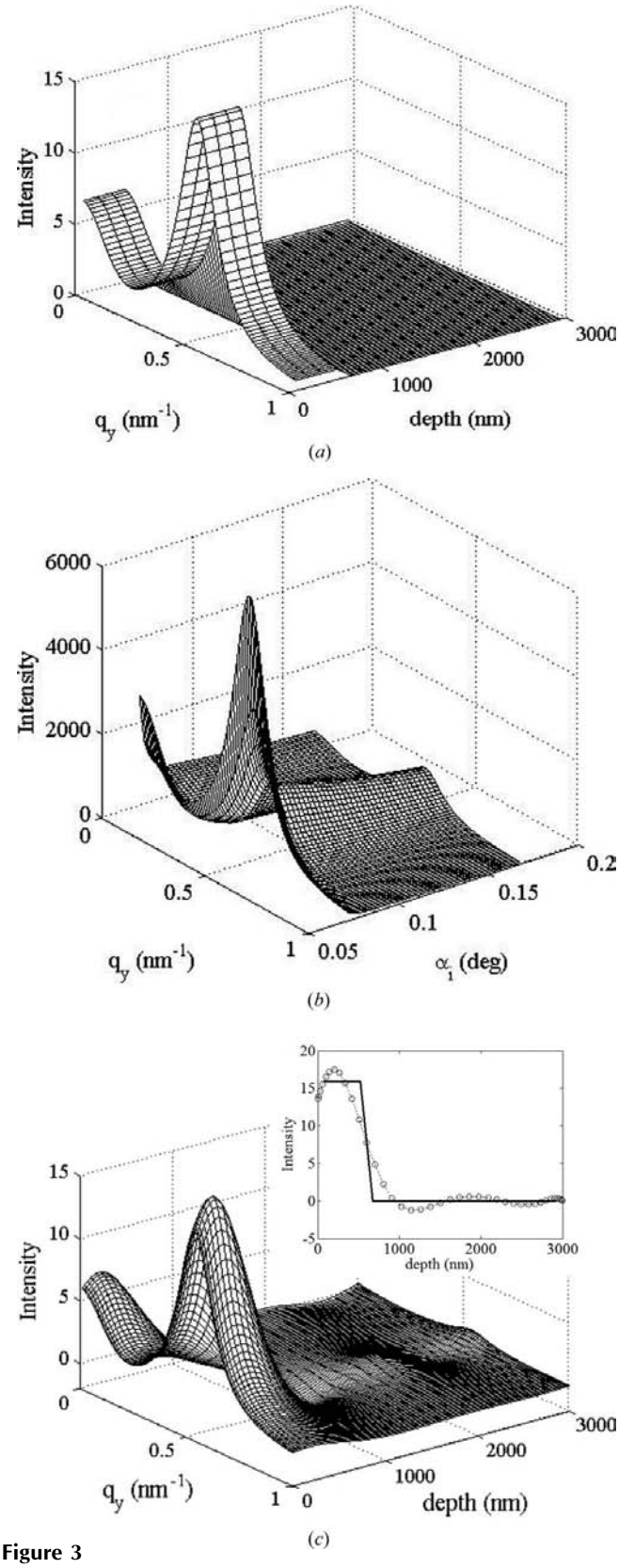

Figure 3
(*a*) Ideal GISAXS profiles for a thin homogeneous film (0.6 µm) as a function of depth below the air–material interface. (*b*) Simulated GISAXS profiles for varying incident angles with the thin film. (*c*) Reconstructed GISAXS profiles as a function of depth below the air–material interface. The inset compares the reconstructed peak amplitude with the ideal amplitude.

for reasonable (within $\pm 0.90D$) estimates of sample thicknesses. Reasonable solutions were not possible for sample thicknesses that were overestimated by more than about 15%. The practical question of identifying the best solution to the ill-posed integral equations (13) and (14) has not yet been thoroughly dealt with through development of a mathematical statement of best-fit criteria (Svergun, 1992). For the purposes of this work, an approximate visual criterion of a non-negative solution without oversmoothing (Broadhurst, Rogers, Lowe & Lane, 2005) resulted in a typical value of $c \simeq 0.1$ in equation (20), yielding the perceived best solution.

For the simplest case of a single homogeneous layer of 3 μm thickness, the simulated measured intensity seen with varying incident angle is shown in Fig. 2(*a*). (Intensity data are given in arbitrary units for all figures.) It is assumed that the substrate is completely homogeneous and does not scatter. Fig. 2(*b*) shows the recovered scattering as a function of q_y in the plane of the sample surface and as a function of $-z$, the depth below the surface. Fig. 3(*a*) demonstrates the case of a thin homogeneous film of thickness 0.6 μm with a single peak located on a layer of 2.4 μm of material of similar μ and no structure. The two layers are separated by an unphysical sharp interface. The simulated observed scattering as a function of incident angle is shown in Fig. 3(*b*). Reconstructed scattering as a function of depth, $-z$, below the sample surface using 40 terms in the collocating polynomial series is shown in Fig. 3(*c*) with the inset indicating the trends of the calculated and known peak intensities. As noted by Broadhurst, Rogers, Lowe & Lane (2005), the presence of a discontinuity in the model system results in oscillations in the recovered intensity in the vicinity of the q_y location of the model peak. Fig. 4(*a*) simulates the observed scattering for a bilayer with an upper layer of thickness 1.2 μm on top of a buried layer of thickness 1.8 μm, the two layers having similar absorption coefficients and different lateral structures. The top layer is assigned a relatively weak interaction peak located at $q_y = 0.2$ nm^{-1} and the buried layer has a more intense peak at 0.5 nm^{-1}. Once again, the two layers are separated by an unphysical sharp interface. Fig. 4(*b*) shows the reconstructed scattering as a function of depth below the surface using 40 terms in the polynomial series while Figs. 4(*c*) and 4(*d*) show the trends of the calculated and known interaction peak intensities for the two

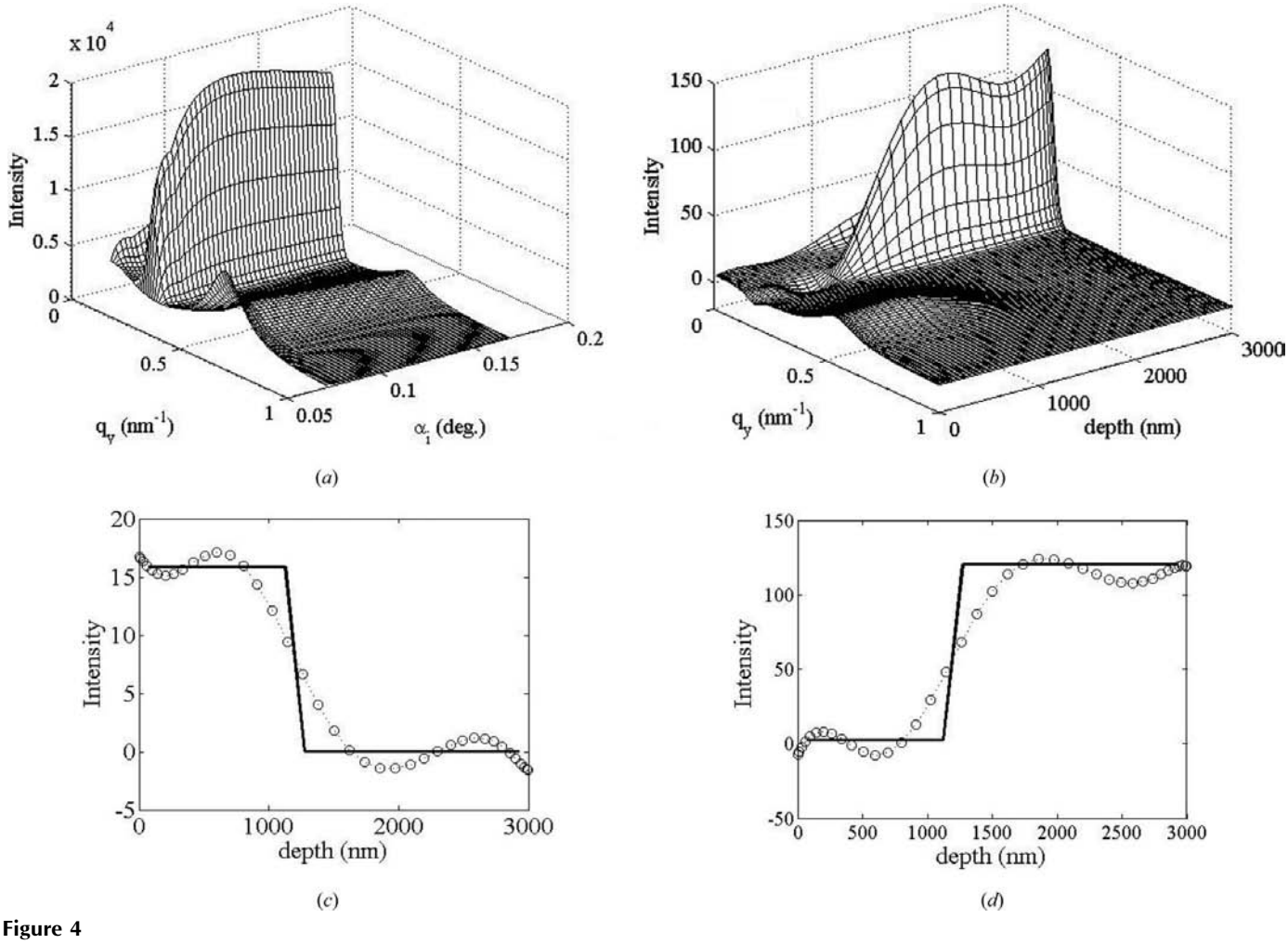

Figure 4
(*a*) Simulated GISAXS profiles for varying incident angles for a bilayer system (1.2 μm on top of 1.8 μm) as a function of depth below the air–material interface. (*b*) Reconstructed GISAXS profiles as a function of depth below the air–material interface. The reconstructed peak amplitudes of (*c*) the upper layer and (*d*) the buried layer are compared with the ideal amplitudes.

layers. The basic ability of the procedure proposed by Broadhurst, Rogers, Lowe & Lane (2005) to recover lateral scattering from buried layers is apparent.

The simulated results presented here demonstrate that the modification to the original numerical method proposed by Broadhurst, Rogers, Lowe & Lane (2005) and Broadhurst, Rogers, Lane & Lowe (2005) is viable without addressing the much more complex question of isolating and correctly processing the reflected source branch of the multiple-scattering processes typically seen with GISAXS data.

3.2. Experimental data

The minimum requirement for a test-case sample is that it exhibits distinctly different GISAXS as a function of depth. In addition, an alternative, direct method of identifying depth-dependent structure as an independent test of the proposed procedure is required. The sample should be thick enough (> 1 μm) to permit differentiation of surface, intermediate bulk and near-substrate in-plane structure. A viable candidate was identified in a blend (50–50 wt%) of poly(*tert*-butyl acrylate-b-methylmethacrylate) (BM) and poly(styrene-b-isoprene) (SI). The polymer samples, purchased from Polymer Source Inc., were synthesized by anionic polymerization. The polydispersity of the BM sample was 1.03 with block number average molecular weights of 18 400 [poly(*tert*-butyl acrylate) (PtBuA)] and 3100 [poly(methyl methacrylate) (PMMA)]. The SI sample polydispersity was given as 1.08 with block number average molecular weights of 36 000 [polystyrene (PS)] and 17 000 [polyisoprene (PI)]. Supported film samples were prepared by first dissolving the combined, as-received polymers in excess dichloromethane to form a 4 wt% (g ml^{-1}) solution. The polymer blend solution (BMSI) was then spin-coated at 500 r.p.m. for 10 s and then at 2500 r.p.m. for 30 s onto cleaned Si(100) wafers (Singh *et al.*, 2007). The polymer film (BMSI) was annealed at 393 K for 12 h in a dry N_2 environment. An average linear absorption coefficient of 2.5×10^{-7} nm^{-1} was estimated for the blend (http://physics.nist.gov/PhysRefData/XrayMassCoef). Cross-sectional scanning electron microscopy (SEM) images of the film structure indicated the presence of a 'bumpy' structure (Fig. 5) similar to that reported by Wang *et al.* (2002) for films of pure PtBuA as a result of AFM measurements. The cause of the observed film structure in this case has not yet been determined. As shown in the inset of Fig. 5, where polymer is identified on the native oxide substrate surface, it appears to be composed of three distinct layers with a thin upper layer at the air interface of about 100 nm in depth and a thicker buried layer at the substrate of about 500 nm.

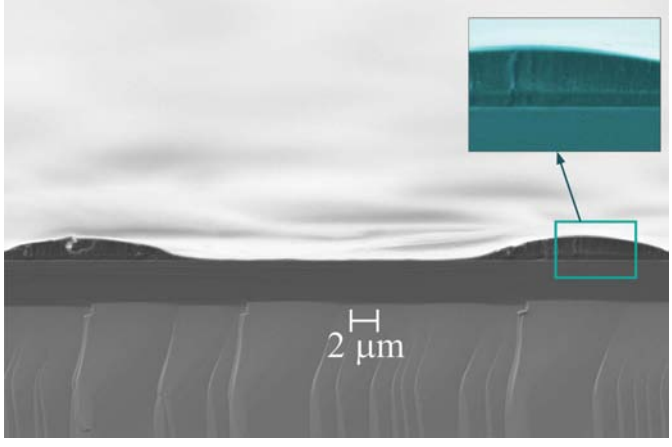

Figure 5
Cross-sectional SEM image of the BMSI polymer blend on the silicon substrate with an inset highlighting the apparent multilayer structure.

GISAXS measurements were performed at D-line of the Cornell High Energy Synchrotron Source (CHESS) at Cornell University in Ithaca, NY, USA, using the sample chamber described by Singh *et al.* (2007). The basic beamline configuration is described elsewhere (Busch *et al.*, 2007). Working with an energy of 10.4 keV, the X-ray beam spot size at the sample was 100 μm (vertical) by 500 μm (horizontal). The sample-to-detector distance was 1830 mm. Final calibration of the two-dimensional charge-coupled device (CCD) detector (1024 by 1024 pixels with a pixel size of 47.2 μm) was performed using a silver behenate standard and found to be 678 pixels per degree. In addition to the usual primary beamstop blocking the direct beam, a vertical strip beamstop was used to protect the CCD detector from the specularly reflected beam. No information on the beam divergence was available. Sample alignment was performed using an ion chamber to measure conventional X-ray reflectivity. The resulting data allowed identification (Busch *et al.*, 2007) of the zero angle ($\alpha_i = 0.0^\circ$), the air–material critical angle and the substrate critical angle. No Kiessig fringes, characteristic of the homogeneous film on the substrate, were resolved, implying that the film was thicker than the estimated 0.3 μm resolution limit of the beamline. The sample was repositioned after alignment and at regular intervals during angle-resolved measurements to ensure reference to fresh sample surface without radiation damage.

Two-dimensional GISAXS profiles of the BMSI film structure at 323 K for varying incident beam angles of α_i = 0.067, 0.080, 0.100 and 0.114° are shown in Fig. 6. Following Fig. 1, the two-dimensional scattering profiles are defined by two perpendicular axes with the in-plane exit angle expressed as 2θ and the out-of-plane exit angle expressed as α_f, relative to the sample surface. It is clear that the lateral structure at Q_z = 0 (the vertical location of the specular beam) varies with angle (penetration depth). An intense primary peak is located at $2\theta \simeq 0.19^\circ$ ($q_y \simeq 0.18$ nm^{-1}), although this is not clearly resolved by the colour map, which is chosen to identify weaker (by two orders of magnitude) higher-order peaks at $2\theta \simeq 0.37$ and 0.49°. The in-plane lateral structure at low α_i with relative peak locations $1{:}4^{1/2}{:}7^{1/2}$ seen in Fig. 6(*a*) is not seen in GISAXS measurements with the bare substrate. In addition, BMSI films prepared from the same solutions using the same spin-coating protocol but with substrates treated to be strongly hydrophobic (Shin *et al.*, 2001) exhibit GISAXS profiles which are similar to Fig. 6(*a*), with three distinct lateral peaks for the full range of incident angles considered; the coalescence of the two higher-order lateral peaks into a single

broad peak at $2\theta \simeq 0.43^\circ$ is not seen at high α_i with hydrophobic substrates. The substrate for the data reported here (Fig. 6) was effectively neutral (not strongly hydrophobic). It is therefore reasonable to assume that the observed scattering is due to the polymer structure and that this structure varies as a function of depth in the sample as well as with the nature of the polymer/substrate interface.

Fig. 7 shows a three-dimensional surface plot of the lateral scattering at high q_y, excluding all scattering associated with reflectivity processes as well as the intense primary peak, for the BMSI sample at 323 K at the specular position ($\alpha_f = \alpha_i$) for varying α_i. The primary peak is excluded to avoid any possible contamination of the lateral scattering data by reflectivity effects. Data were recorded for 24 angles in increments of $0.0025 \pm 0.0005^\circ$. A nominal angular range of 0.0700–0.1275° was used with precise measures of true incident angle obtained upon close inspection of the two-dimensional images. Transmission SAXS data for similar polymer materials were obtained using a conventional X-ray tube with a line-focus Cu $K\alpha$ (8.05 keV) source. Background corrected, binned and desmeared data (Singh *et al.*, 1993) obtained with approximately 5 h exposure times for the pure BM, pure SI and blended BMSI samples are shown in the inset of Fig. 7. The SI sample exhibits a strong primary peak at $q^* = q_y \simeq 0.18\ \mathrm{nm}^{-1}$ and weaker (by about two orders of magnitude) peaks at locations $3^{1/2}q^*{:}4^{1/2}q^*{:}7^{1/2}q^*$ characteristic of a hexagonally ordered structure. Except for the absence of the second lateral peak expected at the $q = 3^{1/2}q^*$ position, the locations and relative intensities of the primary peak and the weak secondary peaks seen with pure SI and the blended BMSI in the bulk phase are consistent with the low α_i GISAXS observations of Fig. 6(*a*). The GISAXS data at the high incident angle of 0.114° (Fig. 6*d*) exhibit the strong primary peak at $q_y \simeq 0.18\ \mathrm{nm}^{-1}$ (not visible in the image) as well as a weaker broad peak at $q_y \simeq 0.4\ \mathrm{nm}^{-1}$. The broad peak may be associated with the presence of pure BM sample structure, although that peak is located at $q_y \simeq 0.5\ \mathrm{nm}^{-1}$ in the bulk phase (Fig. 7). Some distortion can be expected due to the presence of scattering from pure SI (or mixed BMSI) as well as possible interface interaction effects.

The GISAXS data for angles $\alpha_i > \alpha_{c,m}$ at values $q_y > 0$ (excluding all possible reflectivity effects) were corrected for parasitic background and the T_f coefficient of equation (13) ($R_i \simeq 1$). The data were then processed using the algorithm described above to reconstruct the lateral scattering as a function of depth below the surface for values of $-z$ determined by the use of 40 terms in the Chebyshev polynomial series and an estimated total film thickness of 3 µm. Ideally the sample thickness would be a known parameter but, as discussed above, SEM data and X-ray reflectivity were not useful in identifying a well defined value. The choice of 3 µm for the fitting procedure offered the best results in terms of the usual visual criteria of a non-negative solution without oversmoothing. The resulting scattering profiles for the 323 K BMSI sample are shown for a range of depths in Fig. 8(*a*). It is acknowledged that a definite relation between the scattering data and the visual image offered by SEM has not been clearly established. It is, however, clear that angle-resolved GISAXS measurements (Figs. 6 and 7) identify a structure which changes with depth for this sample. In contrast, cross-sectional SEM images of pure styrene–butadiene films (Singh *et al.*, 2007) prepared using similar spin-coating methods did not offer any visual evidence of a multilayer structure and no variation of the observed GISAXS data was observed with varying incident angle for this material, where a random orientation of lamellar domains was identified. The reconstructed depth-specific scattering data for the BMSI sample examined here are roughly consistent with the SEM image of Fig. 5, in that distinct scattering profiles can be associated with the material at both the air (for about 150 nm depth) and the substrate (for about 700 nm depth) interfaces, while the SEM image appears to show distinct upper and lower structures as well. The relative thickness of the interface layers suggested by the SEM image

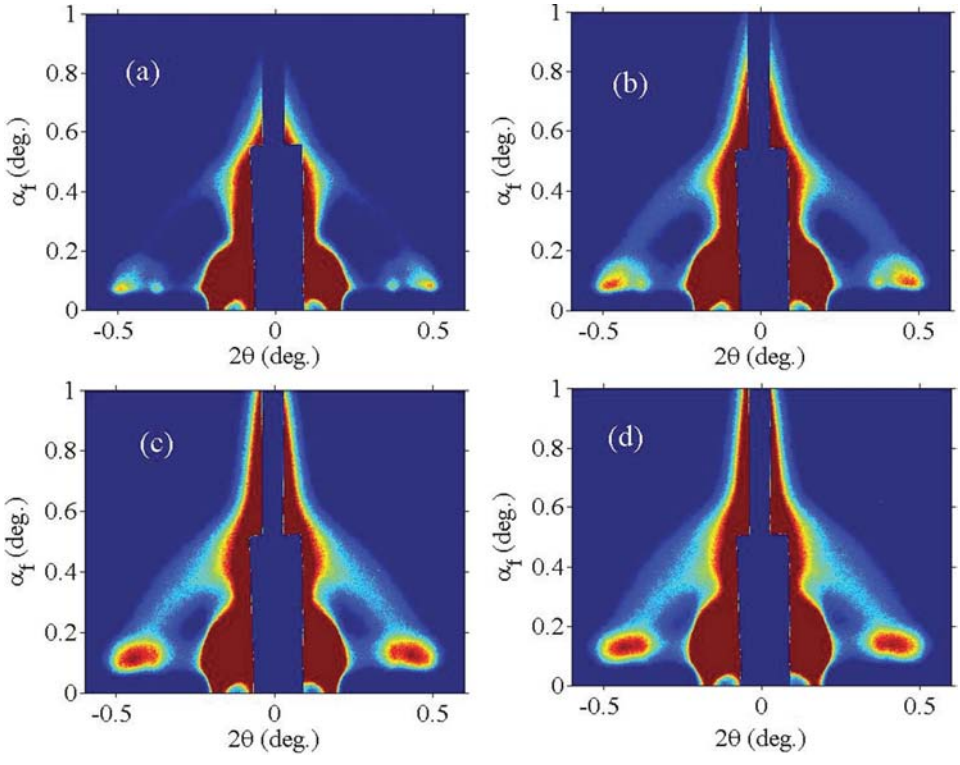

Figure 6
Two-dimensional GISAXS images for the 323 K BMSI polymer at (*a*) $\alpha_i = 0.067^\circ$, (*b*) $\alpha_i = 0.080^\circ$, (*c*) $\alpha_i = 0.100^\circ$ and (*d*) $\alpha_i = 0.114^\circ$.

of Fig. 5 is approximately consistent with the reconstructed data. The depth-profiled data imply that either pure SI or blended BMSI (or both) is located at the air–material interface, while pure BM is located at the substrate interface.

A temperature effect can be clearly identified when comparing Figs. 8(*a*) and 8(*b*). At 323 K (Fig. 8*a*), two distinct peaks associated with the air–material interface are observed at $q_y \simeq 0.345$ nm^{-1} and at 0.450 nm^{-1}. At 473 K (Fig. 8*b*), the air–material interface exhibits a significantly different scattering profile, approaching a broad plateau in the range 0.32–0.43 nm^{-1} rather than a double-peak structure. At 473 K the scattering profile for material at the substrate interface is again distinctly different from that seen for material at the air interface. This scattering is also distinctly different in shape from that seen with the 323 K sample at the same depth. The effect of temperature can also be seen in the differences in the scattering profiles associated with intermediate layers for the two temperatures. Detailed curve fitting of reconstructed scattering profiles to quantify the temperature effect in terms of sample depth is in progress.

Finally, the effect of the enhancement expected as a result of the Fresnel T_f coefficient of equation (13), calculated assuming ideal interfaces possessing no roughness for values of α_i close to $\alpha_{c,m}$, was not clearly observed with these data. Fig. 9 shows the summed intensity values at the specular position for a range of 0.25 nm^{-1} < q_y < 0.62 nm^{-1} with and without correction for the $|T_f|^2$ coefficient. Fig. 10 shows the reconstructed depth-dependent lateral scattering for the 323 K BMSI sample using data that were not corrected for the ideal Fresnel coefficient. The observed trend in the scattering as a function of depth, consistent with a three-layer system, is

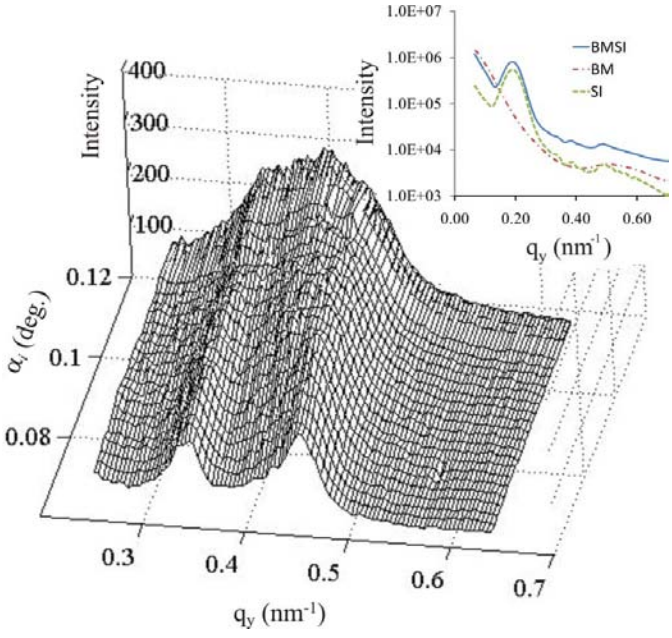

Figure 7
Three-dimensional surface plot of the specular lateral scattering ($\alpha_f = \alpha_i$) for varying α_i with the 323 K BMSI polymer film. The inset shows transmission-mode SAXS data for pure BM, pure SI and blended BMSI samples.

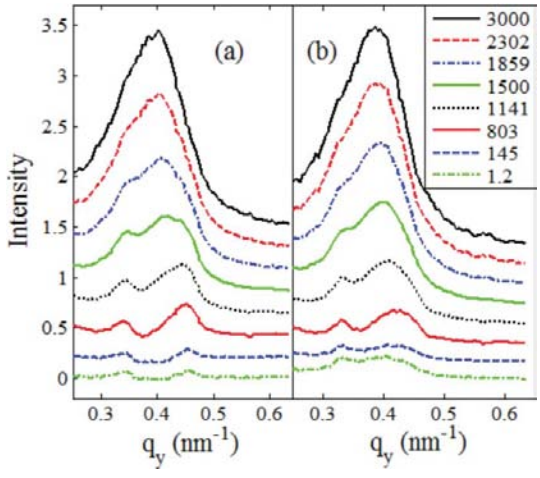

Figure 8
(*a*) Reconstructed lateral scattering profiles for the 323 K BMSI film as a function of depth below the surface. (*b*) Reconstructed lateral scattering profiles for the 473 K BMSI film as a function of depth below the surface. The legend shows the depths in nm.

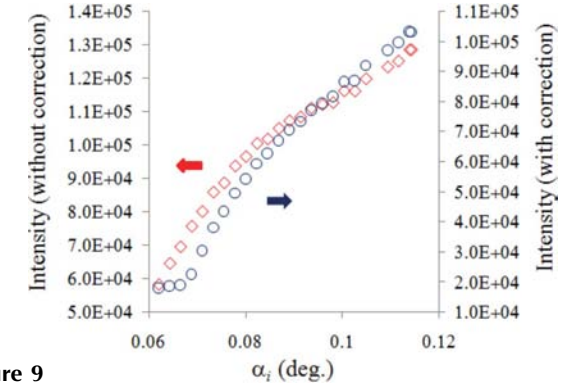

Figure 9
Summed lateral scattering at the specular position for high q_y without (diamonds) and with (circles) correction by the transmission Fresnel coefficient.

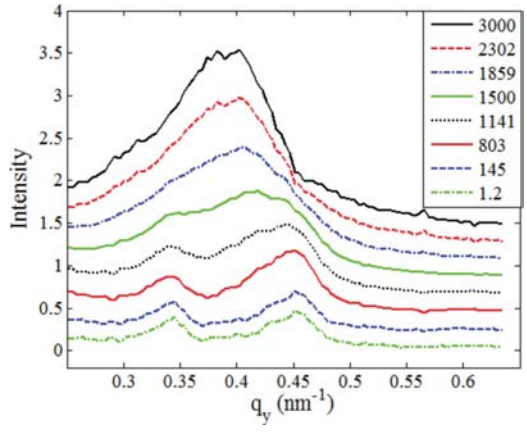

Figure 10
Reconstructed lateral scattering profiles for the 323 K BMSI films as a function of depth below the surface with no correction for the Fresnel coefficient. The legend shows the depths associated with the different scattering profiles in nm.

not obviously affected, suggesting that the proposed procedure, when applied to real systems, is not highly sensitive to amplitude distortions that may result from waveguide effects (Lee *et al.*, 2008) occurring in the region $\alpha_{c,m} < \alpha_i < \alpha_{c,s}$.

4. Discussion and conclusions

In this report, a procedure for adapting a recently proposed depth-profiling algorithm (Broadhurst, Rogers, Lowe & Lane, 2005; Broadhurst, Rogers, Lane & Lowe, 2005) to the task of reconstructing small-angle-scattering profiles as a function of specific depths from incident-angle-resolved GISAXS data has been described. The basic extension of the original method, dealing with reconstruction of scattering normal to the interface with assumed material homogeneity parallel to the surface, to one allowing reconstruction of scattering from lateral inhomogeneities has been tested using simulated data for layered systems. Application to GISAXS data requires a careful consideration of the multiple-scattering processes that have been shown to result from the presence of substrate reflections. The method proposed here is based on the assumptions that scattering relative to the reflected beam can be isolated, that reflectivity effects are removed and that correlations between hypothetical layers introduced by the discretization process can be neglected. Applications to data obtained for a thick polymer film exhibiting distinctly different lateral scattering as a function of incident angle have been used to test the procedure in real systems. The results presented here are intended to serve as a proof of concept of the application of depth-profiling methods to the determination of depth-dependent in-plane scattering profiles of substrate-supported copolymer films. It is acknowledged that the basic implementation of the algorithm can be significantly improved through consideration of a number of features. These include introduction of more sophisticated characterization of the quality of the resulting solution profiles, incorporation of a varying linear absorption coefficient and a better understanding of the role played by the Fresnel transmission function when dealing with non-ideal interfaces. Effective estimates of layer thicknesses with estimated uncertainties have not yet been attempted, given the uncertainty in the true sample thickness and the absence of information on the X-ray source divergence.

In conclusion, the feasibility of extracting depth-specific small-angle-scattering data from GISAXS profiles has been demonstrated. For situations where scattering relative to the specular beam can be isolated, the method offers the possibility of an *in-situ* nondestructive quantitative measure of interface-induced ordering/disordering effects.

The authors thank C. Elliott for SEM measurements and M. S. Müller for his assistance with the GISAXS measurements. We also thank D.-M. Smilgies and the Cornell High Energy Synchrotron Source (CHESS) for providing us with an excellent X-ray source, beamline instrumentation and support. CHESS is a national user facility supported by the National Science Foundation and the National Institute of Health/National Institute of General Medical Sciences under Award DMR-0225180. This work was financially supported by the Natural Sciences and Engineering Research Council of Canada (Discovery Grant No. 46165-03).

References

Als-Nielsen, J. & McMorrow, D. (2001). *Elements of Modern X-Ray Physics*. New York: John Wiley and Sons.
Born, M. & Wolf, E. (1999). *Principles of Optics, Electromagnetic Theory of Propagation, Interference and Diffraction of Light*, 7th ed., ch. XIII. Cambridge University Press.
Boyce, W. E. & DiPrima, R. C. (1997). *Elementary Differential Equations and Boundary Value Problems*. New York: John Wiley and Sons.
Broadhurst, A., Rogers, K. D., Lane, D. W. & Lowe, T. W. (2005). *Powder Diffr.* **20**, 233–240.
Broadhurst, A., Rogers, K. D., Lowe, T. W. & Lane, D. W. (2005). *Acta Cryst.* A**61**, 139–146.
Brown, G. & Chakrabarti, A. (1994). *J. Chem. Phys.* **101**, 3310–3317.
Busch, P., Posselt, D., Smilgies, D.-M., Rauscher, M. & Papadakis, C. M. (2007). *Macromolecules*, **40**, 630–640.
Colombi, P., Zanola, P., Bontempi, E. & Depero, L. E. (2007). *Spectrochim. Acta B*, **60**, 554–557.
David, T., Buttard, D., Schülli, T., Dallhuin, F. & Gentile, P. (2008). *Surf. Sci.* **602**, 2675–2680.
Dietz, D., Zerson, M., Riesch, C., Gigler, A. M., Stark, R. W., Rehse, N. & Magerle, R. (2008). *Appl Phys. Lett.* **92**, 143107.
Dosch, H. (1992). *Critical Phenomena at Surfaces and Interfaces*. Berlin: Springer-Verlag.
Fenter, P. & Park, C. (2004). *J. Appl. Cryst.* **37**, 977–987.
Ferrero, C., Servidori, M., Thiaudière, D., Milita, S., Lequien, S., Sama, S., Setzu, S. & Metzger, T. H. (2003). *J. Electrochem. Soc.* **150**, E366–E370.
Foster, M. D. (1993). *Crit. Rev. Anal. Chem.* **24**, 179–241.
Fruchart, O., Renaud, G., Barbier, A., Noblet, M., Ulrich, O., Deville, J.-P., Scheurer, F., Mane-Mane, J., Repain, V., Baudot, G. & Rousset, S. (2003). *Europhys. Lett.* **63**, 275–281.
Gibaud, A., Grosso, D., Smarsly, B., Baptiste, A., Bardeau, J. F., Babonneau, F., Doshi, D. A., Chen, Z., Jeffrey Brinker, C. & Sanchez, C. (2003). *J. Phys. Chem. B*, **107**, 6114–6118.
Hamley, I. W. (1998). *The Physics of Block Copolymers*. New York: Oxford University Press.
Heo, K., Yoon, J., Jin, S., Kim, J., Kim, K.-W., Shin, T. J., Chung, B., Chang, T. & Ree, M. (2008). *J. Appl. Cryst.* **41**, 281–291.
Kawaguchi, D., Tanaka, K., Kajiyama, T., Takahara, A. & Tasaki, S. (2003). *Macromolecules*, **36**, 1235–1240.
Kitano, H., Akasaka, S., Inoue, T., Chen, F., Takenaka, M., Hasegawa, H., Yoshida, H. & Nagano, H. (2007). *Langmuir*, **23**, 6404–6410.
Kötschau, I. M. & Schock, H. W. (2006). *J. Appl. Cryst.* **39**, 683–696.
Lee, B., Lo, C.-T., Thiyagarajan, P., Lee, D. R., Niu, Z. & Wang, Q. (2008). *J. Appl. Cryst.* **41**, 134–142.
Lee, B., Park, I., Park, H., Lo, C.-T., Chang, T. & Winans, R. E. (2007). *J. Appl. Cryst.* **40**, 496–504.
Lee, B., Park, I., Yoon, J., Park, S., Kim, J., Kim, K.-W., Chang, T. & Ree, M. (2005). *Macromolecules*, **38**, 4311–4323.
Lee, B., Yoon, J., Oh, W., Hwang, Y., Heo, K., Jin, K. S., Kim, J., Kim, K.-W. & Ree, M. (2005). *Macromolecules*, **38**, 3395–3405.
Leroy, F., Renaud, G., Létoublon, A., Rohart, S., Girard, Y., Repain, V., Rousset, S., Coati, A. & Garreau, Y. (2008). *Phys. Rev. B*, **77**, 045430.
Luo, J. & Tao, K. (1996). *Thin Solid Films*, **279**, 53–58.

Metwalli, E., Couet, S., Schlage, K., Röhlsberger, R., Körstgens, V., Ruderer, M., Wang, W., Kaune, G., Roth, S. V. & Müller-Buschbaum, P. (2008). *Langmuir*, **24**, 4265–4272.
Müller-Buschbaum, P. (2003). *Anal. Bioanal. Chem.* **376**, 3–10.
Naudon, A., Slimani, T. & Goudeau, P. (1991). *J. Appl. Cryst.* **24**, 501–508.
Neerinck, D. G. & Vink, T. J. (1996). *Thin Solid Films*, **278**, 12–17.
Pfeiffer, F., Zhang, W. & Robinson, I. K. (2004). *Appl. Phys. Lett.* **84**, 1847–1849.
Press, W. H., Teukolsky, S. A., Vetterling, W. T. & Flannery, B. P. (1992). *Numerical Recipes in Fortran*, 2nd ed., ch. 18. New York: Cambridge University Press.
Reichert, H., Honkimäki, V., Snigirev, A., Engemann, S. & Dosch, H. (2003). *Physica B*, **336**, 46–55.
Robinson, I. K., Tabuchi, M., Hisadome, S., Oga, R. & Takeda, Y. (2005). *J. Appl. Cryst.* **38**, 299–305.
Schlepütz, C. M., Herger, R., Willmott, P. R., Patterson, B. D., Bunk, O., Brönnimann, Ch., Henrich, B., Hülsen, G. & Eikenberry, E. F. (2005). *Acta Cryst.* A**61**, 418–425.
Shin, K., Hu, X., Zheng, X., Rafailovich, M. H., Sokolov, J., Zaitsev, V. & Schwarz, S. A. (2001). *Macromolecules*, **34**, 4993–4998.
Singh, M. A., Ghosh, S. S. & Shannon, R. F. (1993). *J. Appl. Cryst.* **26**, 787–794.
Singh, M. A., Groves, M. N., Müller, M. S., Stahlbrand, I. J. & Smilgies, D.-M. (2007). *Rev. Sci. Instrum.* **78**, 113910.
Stein, G. E., Kramer, E. J., Li, X. & Wang, J. (2007). *Macromolecules*, **40**, 2453–2460.
Svergun, D. I. (1992). *J. Appl. Cryst.* **25**, 495–503.
Vartanyants, I. A., Grigoriev, D. & Zozula, A. V. (2007). *Thin Solid Films*, **515**, 5546–5552.
Wang, X. P., Loy, M. M. T. & Xiao, X. (2002). *Nanotechnology*, **13**, 478–483.